Exploring the coordination capabilities of a family of flexible benzotriazole-based ligands using Cobalt (II) sources

Article (Accepted Version)

Exploring the coordination capabilities of a family of flexible benzotriazole-based ligands using Cobalt (II) sources

Edward Loukopoulos,[a] Nicholas F. Chilton,[b] Alaa Abdul-Sada,[a] and George E. Kostakis*[a]

[a] Department of Chemistry, School of Life Sciences, University of Sussex, Brighton BN1 9QJ, United Kingdom. E-mail: G.Kostakis@sussex.ac.uk

[b] School of Chemistry, The University of Manchester, Manchester M13 9PL, United Kingdom

RECEIVED DATE (to be automatically inserted after your manuscript is accepted if required according to the journal that you are submitting your paper to)

Running Title : Cobalt benzotriazole coordination compounds

* Corresponding authors

ABSTRACT

In this study we focus on the coordination chemistry of a family of three flexible benzotriazole-based ligands (L^1-L^3) using Cobalt(II) salts. Our efforts have resulted to the formation of ten novel compounds, formulated as $[Co_2(L^1)_2Cl_4]\cdot 2MeCN$ (**1**·2MeCN), $Co_2(L^1)_2Br_4$ (**2**), $[Co(L^2)Cl_2]\cdot MeCN$ (**3**·MeCN), $Co(L^2)Cl_2$ (**4**), $[Co_2(L^2)_2Br_4]\cdot 2MeCN$ (**5**·2MeCN), $[Co(L^2)_2(NO_3)_2]\cdot 2MeCN$ (**6**·2MeCN), $[Co_2(L^3)_2Cl_4]\cdot 2MeCN$ (**7**·2MeCN), $Co_2(L^3)_2Cl_4$ (**8**), $Co_2(L^3)_2Br_4$ (**9**), and $Co(L^3)_2(NO_3)_2$ (**10**). The structures have been well characterised through X-Ray crystallography, FT-IR, ESI-MS, PXRD, Elemental Analysis and TGA studies. The compounds show a large structural variety depending on synthetic parameters (ratio, temperature and metal salt) and the ligand selection (various conformations in each ligand). When tuned appropriately, these factors drastically affect dimensionality, metal geometry and the nuclearity of the final product, resulting in a range of 0D dimers (**1**, **3**, **5**, **8**, **9**), 1D (**2**, **7**, **10**) and 2D (**4**, **6**) coordination polymers (CPs). A temperature-induced single-crystal to single-crystal transformation of compound **3** to **4** is additionally reported. The magnetic properties of representative compounds (**4**, **7**, **9**) are subject to large changes with only minor structural variations, suggesting that tetrahedral Co(II) nodes in CPs or MOFs could function as sensitive reporters of small changes in the local environment.

KEYWORDS : Cobalt, benzotriazole, coordination chemistry, magnetism,

INTRODUCTION

The assembly of polytopic organic ligands and metal centers yields coordination polymers (CPs) and metal organic frameworks (MOFs), many of which find applications in conductivity,[1] catalysis,[2] magnetism,[3] gas sorption,[4] biological sensing[5] and luminescence.[6] The structure and topology of CPs may be manipulated by changing the reaction conditions, leading to a large variety of structurally and topologically unique products.[7–9] However, controlling and predicting the final outcome of the self-assembly procedure remains one of the major challenges in the field.[10] The final products are often strongly influenced by factors such as the behavior of a functional group in a molecule,[11] the influence of the crystallization conditions and the various conformations of the components within the crystal.[12]

For many years, the synthesis of CPs or MOFs was conducted almost entirely using rigid bridging ligands.[13] This played a vital role in their thermal stability and made the prediction of final structures easier.[14,15] Nevertheless, despite the challenges they pose, flexible ligands are also being used in recent years to generate frameworks.[13,16–22] The conformational freedom of the ligand backbone allows the network to respond reversibly to the presence or absence of guest molecules,[23] however the downside is the increased possibility of forming more than one products. The middle ground between these two extremes is to employ semi-rigid ligands with a smaller degree of flexibility, which have also been successfully employed to afford porous networks.[24–31]

Benzotriazole and its derivatives have been frequently employed in the construction of CPs and MOFs[32–44] as well as polynuclear coordination clusters (CCs).[45–48] Its multi-modal coordination ability, through the 1,2,3-triazole moiety, provides enormous versatility when combined with transition metal ions.[49] We therefore sought to explore the potential of semi-rigid ligands in the field of CPs, in conjunction with the coordination capabilities of benzotriazole. Our initial studies reported the synthesis and characterization of several coordination compounds using semi-rigid benzotriazole-based ligands, as well as their catalytic potential in various reactions.[50–52]

On the other hand, it is well known that Co^{II} can adopt versatile coordination geometries, and often displays large magnetic anisotropy.[53–55] Furthermore, detailed studies of the correlation between the coordination geometry of the metal center and the magnetic parameters of the compounds has already been well established, especially for tetra-[56–59], penta-[60–62] and hexa-coordinated[63,64] Co^{II} complexes.

Encouraged by these results, we herein employ a family of benzene-substituted benzotriazole molecules, namely 1,4-bis((1H-benzo[d][1,2,3]triazol-1-yl)methyl)benzene (L^1), 1,3-bis((1H-benzo[d][1,2,3]triazol-1-yl)methyl)benzene (L^2), and 1,2-bis((1H-benzo[d][1,2,3]triazol-1-yl)methyl)benzene (L^3) (Scheme 1). These ligands have been scarcely used in coordination chemistry;[51,52,65,66] they contain a flexible C-N bond in an otherwise rigid molecule and when coupled with different positions on the benzene ring (para-, meta- and ortho-substitution for L^1, L^2 and L^3, respectively), can lead to a wide array of coordination motifs. The present work aims to study the coordination capabilities of L^1, L^2, L^3 along with Co^{II} salts as metal sources, thus we found that subtle changes in the synthetic protocol (ratio, temperature, salt) result in drastic changes to the dimensionality and the nuclearity of the final product. Herein we report ten new compounds, formulated as $[Co_2(L^1)_2Cl_4]\cdot 2MeCN$ (**1**·2MeCN), $Co_2(L^1)_2Br_4$ (**2**), $[Co(L^2)Cl_2]\cdot MeCN$ (**3**·MeCN), $Co(L^2)Cl_2$ (**4**), $[Co_2(L^2)_2Br_4]\cdot 2MeCN$ (**5**·2MeCN), $[Co(L^2)_2(NO_3)_2]\cdot 2MeCN$ (**6**·2MeCN), $[Co_2(L^3)_2Cl_4]\cdot 2MeCN$ (**7**·2MeCN), $Co_2(L^3)_2Cl_4$ (**8**), $Co_2(L^3)_2Br_4$ (**9**), and $Co(L^3)_2(NO_3)_2$ (**10**). The magnetic properties of **4**, **7** and **9** have been investigated as representative examples of varying connectivity, dimensionality and local nuclearity.

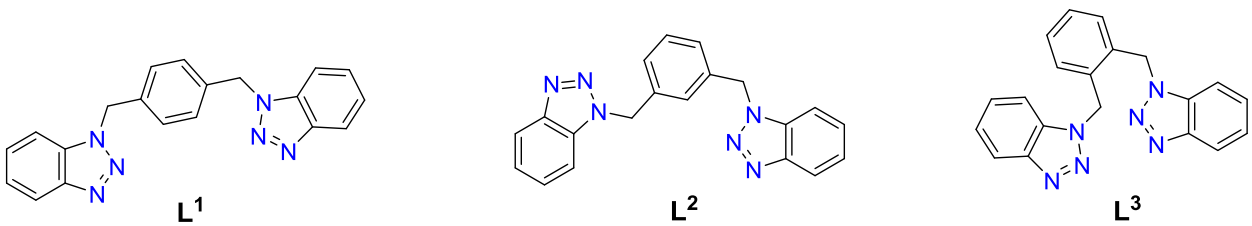

Scheme 1. The organic ligands L^1, L^2, and L^3 used in this study.

EXPERIMENTAL SECTION

Materials. Chemicals (reagent grade) were purchased from Sigma Aldrich and Alfa Aesar. All experiments were performed under aerobic conditions using materials and solvents as received. The ligand 1,2-bis((1H-benzo[d][1,2,3]triazol-1-yl)methyl)benzene (L^3) was synthesized according to the literature method.[49]

Instrumentation. IR spectra of the samples were recorded over the range of 4000-650 cm^{-1} on a Perkin Elmer Spectrum One FT-IR spectrometer fitted with a UATR polarization accessory. EI-MS was performed on a VG Autospec Fissions instrument (EI at 70 eV). NMR spectra were measured on a Varian VNMRS solution-state spectrometer at 500 MHz at 30°C using residual isotopic solvent (DMSO-d_5, δ_H= 2.50 ppm) as internal reference. Chemical shifts are quoted in parts per million (ppm). Coupling constants (J) are recorded in Hertz (Hz). TGA analysis was performed on a TA Instruments Q-50 model (TA, Surrey, UK) under nitrogen and at a scan rate of 10 °C/min. X-ray powder diffraction patterns were recorded at the University of Cyprus.

Magnetic studies. Magnetization data were measured on a Quantum Design MPMS-XL7 SQUID magnetometer. Ground polycrystalline samples were restrained with eicosane in a gelatin capsule at the center of a straw and fixed to the sample rod. Susceptibility measurements were conducted upon cooling the sample in a magnetic field.

Electron paramagnetic resonance. EPR spectra were collected with a Bruker EMX spectrometer at X-band and Q-band, using liquid helium with an Oxford Instruments temperature controller.

Synthetic part. Synthesis of L^1. Benzotriazole (5.0 g, 42.0 mmol) was dissolved in acetone (50 mL) and then potassium carbonate (12.0 g, 86.2 mmol) and potassium iodide (0.50 g, 3.01 mmol) were added. After stirring for 30 min, solid α,α'-dichloro-p-xylene (3.5 g, 20.0 mmol) was added slowly. The mixture was refluxed for 1 h. After cooling, the solution was filtered and the filtrate evaporated to dryness to give a white solid product. The residue was recrystallized from methanol/water (1:1) to give a white

microcrystalline material. Yield: 63%. Selected IR peaks (cm^{-1}): 3065 (w), 3033 (w), 1940 (w), 1615 (m), 1564 (m), 1495 (m), 1455 (m), 1410 (m), 1322 (m), 1312 (m), 1272 (m), 1222 (m), 1150 (m), 1085 (w), 1050 (w), 1000 (m), 981 (w), 966 (m), 944 (m), 906 (m), 837 (m), 787 (m), 762 (m), 740 (s), 733 (s), 696 (m), 667 (m). ^{1}H NMR (500 MHz, DMSO-d_6) δ 8.03 (d, *J* = 8.3 Hz, 2H), 7.39 (s, 4H), 7.37 – 7.29 (m, 6H), 5.96 (s, 4H). ^{13}C NMR (126 MHz, DMSO-d_6) δ 145.80, 144.36, 136.45, 135.56, 133.12, 129.25, 128.63, 128.54, 127.89, 126.91, 124.46, 119.67, 118.29, 111.05, 59.58, 51.05. The results are in agreement to those in the literature.[67] ESI–MS: 379.10 m/z [$C_{20}H_{16}N_6$+K].

Synthesis of L^2. L^2 was prepared in the same method and ratio as L^1, using α,α'-dichloro-m-xylene (3.5 g, 20.0 mmol) after stirring, then refluxing the mixture for 3 h. Yield: 74%. Selected IR peaks (cm^{-1}): 3067 (w), 3034 (w), 1940 (w), 1614 (m), 1588 (w), 1565 (m), 1496 (m), 1453 (m), 1342 (w), 1310 (m), 1274 (m), 1226 (m), 1157 (m), 1105 (w), 1080 (w), 1050 (w), 1000 (m), 981 (w), 954 (m), 850 (m), 780 (m), 739 (s), 702 (m), 665 (m). ^{1}H NMR (500 MHz, DMSO-d_6) δ 8.03 (d, J = 8.3 Hz, 2H), 7.70 (d, J = 8.3 Hz, 2H), 7.44 (t, *J* = 8.2 Hz, 2H), 7.38 – 7.33 (m, 3H), 7.23 (d, *J* = 7.9 Hz, 2H), 5.92 (s, 4H). ^{13}C NMR (126 MHz, DMSO-d_6) δ 145.71, 136.89, 133.01, 129.79, 127.97, 127.85, 127.64, 124.49, 119.64, 110.97, 51.15. The results are in agreement to those in the literature.[68] ESI–MS: 341.15 m/z [$C_{20}H_{16}N_6$+H], 379.10 m/z [$C_{20}H_{16}N_6$+K].

Synthesis of $[Co_2(L^1)_2Cl_4]\cdot 2MeCN$ (**1**·2MeCN). *Method 1*: 0.12 mmol (0.041 g) of L^1 were dissolved in 10 ml MeCN while stirring to produce a colorless solution. A solution containing 0.12 mmol (0.016 g) of anhydrous $CoCl_2$ in MeCN (7.5 ml) was slowly added. The resulting dark blue solution was filtrated, then layered over 10 ml of Et_2O. Blue prismatic crystals were obtained after 2 days. Selected IR peaks (cm^{-1}): 2996 (w), 1595 (w), 1493 (w), 1456 (m), 1439 (w), 1315 (m), 1278 (w), 1226 (m), 1167 (w), 1142 (w), 1104 (w), 1003 (w), 954 (w), 850 (w), 782 (m), 749 (s), 669 (m). Yield: 20% (based on Co). Elemental analysis for $C_{44}H_{38}Cl_4Co_2N_{14}$: C 51.69, H 3.75, N 19.17; found C 51.70, H 3.82, N 19.13.

Alternative Methods: **1** may also be prepared in the same method as above but using either a 2:1 or 1:2 metal:ligand (M:L) ratio.

Synthesis of $Co_2(L^1)_2Br_4$ (**2**). *Method 1*: 0.12 mmol (0.041 g) of L^1 were dissolved in 10 ml Me_2CO while stirring to produce a colorless solution. A solution containing 0.12 mmol (0.027 g) of anhydrous $CoBr_2$ in Me_2CO (7.5 ml) was slowly added. The resulting blue solution was stirred for 45 minutes, while heated to 50°C. After the solution was left to cool, it was filtrated and then carefully layered over 10 ml of Et_2O. Blue needles were obtained after 2 days. Selected IR peaks (cm^{-1}): 3033 (w), 1591 (w), 1495 (w), 1455 (m), 1430 (w), 1313 (m), 1283 (w), 1225 (m), 1180 (w), 1139 (w), 1109 (w), 1002 (w), 963 (w), 836 (w), 772 (m), 734 (s), 669 (m). Yield: 14% (based on Co). Elemental analysis for $C_{40}H_{32}Br_4Co_2N_{12}$: C 42.97, H 2.88, N 15.03; found C 42.99, H 2.92, N 14.93. *Alternative Methods*: **2** is also obtained by performing the same reaction in a 2:1 M:L ratio. It may also be prepared in a similar fashion using MeCN instead of Me_2CO.

Synthesis of $[Co(L^2)Cl_2]\cdot MeCN$ (**3**·MeCN). *Method 1*: 0.12 mmol (0.041 g) of L^2 were dissolved in 10 ml MeCN while stirring to produce a colorless solution. A solution containing 0.24 mmol (0.032 g) of anhydrous $CoCl_2$ in MeCN (7.5 ml) was slowly added. The resulting dark blue solution was filtrated, then subjected to slow evaporation. Blue block crystals were obtained 1 day later. Selected IR peaks (cm^{-1}): 2986 (w), 1592 (w), 1492 (w), 1454 (m), 1315 (m), 1279 (w), 1227 (m), 1167 (w), 1122 (m), 1004 (w), 982 (w), 849 (w), 768 (m), 743 (s), 700 (m). Yield: 52% (based on Co). Elemental analysis for $C_{22}H_{19}Cl_2CoN_7$: C 51.69, H 3.75, N 19.17; found C 51.57, H 3.73, N 19.25. *Method 2*: The product may also be obtained performing a similar reaction in a 1:1 M:L ratio.

Synthesis of $[Co(L^2)Cl_2]$ (**4**). *Method 1*: 0.12 mmol (0.041 g) of L^2 and 0.24 mmol (0.032 g) of anhydrous $CoCl_2$ were dissolved in 12 ml MeCN while stirring to produce a blue solution. After a further 15 minutes of stirring, the solution was stored in a glass vessel and heated at 75 °C for 18 hours to produce large blue block crystals. *Method 2*: **4** may also be obtained by a similar solvothermal reaction in a 1:1 M:L ratio, heating the solution at 100 °C for 3 days. Selected IR peaks (cm^{-1}): 2990 (w), 1594 (w), 1493 (w),

1457 (m), 1314 (m), 1287 (w), 1229 (m), 1167 (w), 1139 (w), 1124 (m), 1093 (w), 1003 (w), 982 (w), 851 (w), 823 (w), 768 (m), 750 (s), 739 (s), 702 (m). Yield: 69% (based on Co). Elemental analysis for $C_{20}H_{16}Cl_2CoN_6$: C 51.09, H 3.43, N 17.87; found C 50.97, H 3.53, N 17.75.

Synthesis of $[Co_2(L_2)_2Br_4]\cdot 2MeCN$ (**5**·2MeCN). **5** was prepared in the same solvent and crystallizing method as **3** (*Methods 1, 2*), using $CoBr_2$ as the metal salt. Selected IR peaks (cm^{-1}): 3055 (w), 1594 (w), 1493 (w), 1456 (m), 1324 (m), 1283 (w), 1224 (m), 1170 (w), 1148 (m), 1002 (w), 972 (w), 779 (m), 765 (m), 747 (s), 702 (m), 672 (m). Yield: 49% (based on Co). Elemental analysis for $C_{44}H_{38}Br_4Co_2N_{14}$: C 44.03, H 3.19, N 16.33; found C 43.90, H 3.12, N 16.20.

Synthesis of $[Co(L^2)_2(NO_3)_2]\cdot 2MeCN$ (**6**·2MeCN). 0.12 mmol (0.041 g) of L^2 and 0.36 mmol (0.105 g) of $Co(NO_3)_2\cdot 6H_2O$ were dissolved in 8 ml MeCN while stirring to produce a pink solution. After a further 15 minutes of stirring, the solution was filtrated, then stored in a glass vessel and heated at 100 °C for 3 days to produce pink block crystals. Selected IR peaks (cm^{-1}): 3038 (w), 1978 (w), 1612 (m), 1596 (m), 1497 (m), 1445 (m), 1370 (m), 1321 (m), 1298 (s), 1226 (m), 1168 (m), 1145 (w), 1128 (m), 1028 (m), 1011 (w), 959 (m), 935 (w), 857 (m), 817 (m), 760 (s), 743 (s), 701 (m), 670 (m). Yield: 22% (based on Co). Elemental analysis for $C_{44}H_{38}CoN_{16}O_6$: C 55.88, H 4.05, N 23.69; found C 55.68, H 3.63, N 22.74.

Synthesis of $[Co_2(L^3)_2Cl_4]\cdot 2MeCN$ (**7**·2MeCN). *Method 1*: **7** was prepared in the same method, ratios and crystallization technique as **1**, using L^3 instead of L^1. Blue prismatic crystals were obtained after 2 days. *Method 2*: **7** was also prepared using the same method and solvothermal conditions as **4** (*Method 1*), in a 1:1, 2:1 or 1:2 ratio, employing L^3 instead of L^2. Selected IR peaks (cm^{-1}): 2974 (w), 2861 (w), 1593 (w), 1491 (w), 1455 (m), 1319 (m), 1285 (w), 1228 (m), 1167 (w), 1151 (w), 1116 (m), 1094 (w), 1002 (w), 959 (w), 846 (w), 814 (w), 790 (w), 765(m), 746 (s), 733 (s), 668 (m). Yield: 64% (based on Co). Elemental analysis for $C_{22}H_{19}Cl_2CoN_7$: C 51.69, H 3.75, N 19.17; found C 49.70, H 3.64, N 17.07. This result corresponds to the loss of one acetonitrile molecule and the presence of one water molecule: $C_{20}H_{16}CoN_6(H_2O)$: C 49.20, H 3.72, N 17.19.

Synthesis of $Co_2(L^3)_2Cl_4$ (**8**). 0.12 mmol (0.041 g) of L^3 and 0.36 mmol (0.048 g) of anhydrous $CoCl_2$ were dissolved in 8 ml MeCN while stirring to produce a blue solution. After a further 15 minutes of stirring, the solution was filtrated, then stored in a glass vessel and heated at 75 °C for 18 hours to produce good quality blue block crystals. Selected IR peaks (cm^{-1}): 2983 (w), 1595 (w), 1497 (w), 1458 (m), 1433 (w), 1323 (m), 1282 (w), 1226 (m), 1171 (w), 1151 (w), 1005 (w), 973 (w), 957 (w), 845 (w), 793 (m), 774 (m), 742 (s), 705 (m), 667 (m). Yield: 60% (based on Co). Elemental analysis for $C_{40}H_{32}Cl_4Co_2N_{12}$: calcd. C 51.09, H 3.43, N 17.87; found C 51.19, H 3.46, N 17.99.

Synthesis of $Co_2(L^3)_2Br_4$ (**9**). **9** was prepared in the same method, ratios and crystallization technique as (**1**), using anhydrous $CoBr_2$ as the metal salt and L^3 instead of L^1. Blue prismatic crystals were obtained after 3 days. Selected IR peaks (cm^{-1}): 3097 (w), 1591 (w), 1493 (w), 1456 (m), 1329 (m), 1281 (w), 1230 (m), 1168 (w), 1143 (m), 1002 (w), 967 (w), 841 (w), 792 (w), 780 (m), 767 (m), 742 (s), 712 (m), 669 (m). Yield: 60% (based on Co). Elemental analysis for $C_{40}H_{32}Br_4Co_2N_{12}$: calcd. C 42.97, H 2.88, N 15.03; found C 42.89, H 2.82, N 14.95.

Synthesis of $Co(L^3)_2(NO_3)_2$ (**10**). **10** was prepared in the same method and ratios as **1**, using $Co(NO_3)_2{\cdot}6H_2O$ as the metal salt and L^3 instead of L^1. The resulting light red solution was filtrated, then kept at a stored vial in room temperature. Pink needle-like crystals were obtained after 3 days. Selected IR peaks (cm^{-1}): 3105 (w), 3081 (w), 1978 (w), 1611 (m), 1592 (m), 1497 (m), 1436 (m), 1374 (m), 1320 (m), 1300 (m), 1279 (m), 1232 (m), 1167 (m), 1145 (m), 1088 (w), 1028 (w), 1003 (m), 970 (m), 953 (m), 930 (w), 857 (m), 814 (m), 755 (s), 741 (s), 711 (m), 669 (m). Yield: 42% (based on Co). Elemental analysis for $C_{40}H_{32}CoN_{14}O_6$: C 55.63, H 3.73, N 22.70; found C 55.62, H 3.64, N 22.79.

X-ray Crystallography. Data for compounds **1**, **3-10** were collected (ω- scans) at the University of Sussex using an Agilent Xcalibur Eos Gemini Ultra diffractometer with CCD plate detector under a flow of nitrogen gas at 173(2) K (for compounds **1**, **3**, **5-10**) or 293 K (compound **4**) using either Mo Kα (λ = 0.71073 Å) or Cu Kα radiation (λ = 1.54184 Å). CRYSALIS CCD and RED software was used respectively for data collection and processing. Reflection intensities were corrected for absorption by

the multi-scan method. Data for **2** were collected at the National Crystallography Service, University of Southampton.[69] All structures were determined using Olex2[70], solved using either Superflip[71] or SHELXT[72,73] and refined with SHELXL-2014.[74] All non-H atoms were refined with anisotropic thermal parameters, and H-atoms were introduced at calculated positions and allowed to ride on their carrier atoms. Crystal data and structure refinement parameters for all compounds are given in Tables S1 and S2. Geometric/crystallographic calculations were performed using PLATON[75], Olex2[70], and WINGX[72] packages; graphics were prepared with Crystal Maker and MERCURY.[76] Each of the crystal structures has been deposited at the CCDC 1531738-1531747.

RESULTS AND DISCUSSION

Crystal Structure Description. Compound **1** crystallizes in the triclinic $P\bar{1}$ space group. The asymmetric unit consists of one Co^{II} center, one L^1 molecule, two chlorine atoms which act as terminal ligands and an acetonitrile molecule in the lattice. X-Ray data further reveal that the structure is finite and does not extend to any dimension (Figure 1, upper). Co^{II} is coordinated to four atoms (Cl1, Cl2, N3, N6) and exhibits a slightly distorted tetrahedral geometry. In this case, the ligand adopts a boat conformation, and its coordination mode is presented in Scheme 2 (Mode A). The mean Co1-N3 and Co1-N6 distances are 2.047(4) and 2.042(4) Å respectively, while the angles of the tetrahedron range from 105.85(12)° to 113.694(14)°. The Co-Cl1 and Co-Cl2 distances were measured at 2.2439(14) and 2.2393(13) Å. Finally, Co···Co distance was found to be 11.5929(19) Å. While no hydrogen bonds are formed, the supramolecular architecture of the complex is formed and stabilized through inter-molecular π···π stacking interactions of the benzotriazole aromatic rings (Figure S1). The values for these interactions are detailed in Table S3.

Similarly to **1**, compound **2** crystallizes in the triclinic $P\bar{1}$ space group and contains one molecule in the asymmetric unit. The unit contains one Co^{II} center, one L^1 molecule and two bromide atoms which act as terminal ligands. The N_2Br_2 coordination environment around the Co^{II} center can be described as

a slightly distorted tetrahedral, in which the angles of the tetrahedron range from 106.27(16)° to 112.77(5)°. Although the metal is coordinated to the ligand through the same N atom as in **1**, in this case the ligand adopts a chair conformation (Scheme 2, Mode B). As a result, the structure is extended infinitely into one direction, forming a one-dimensional coordination polymer (Figure 1, lower). The Co-N and Co-Br distances are 2.021(5) and 2.030(5), 2.3709(10) and 2.3745(10) Å respectively. No hydrogen bonds or other supramolecular interactions were observed.

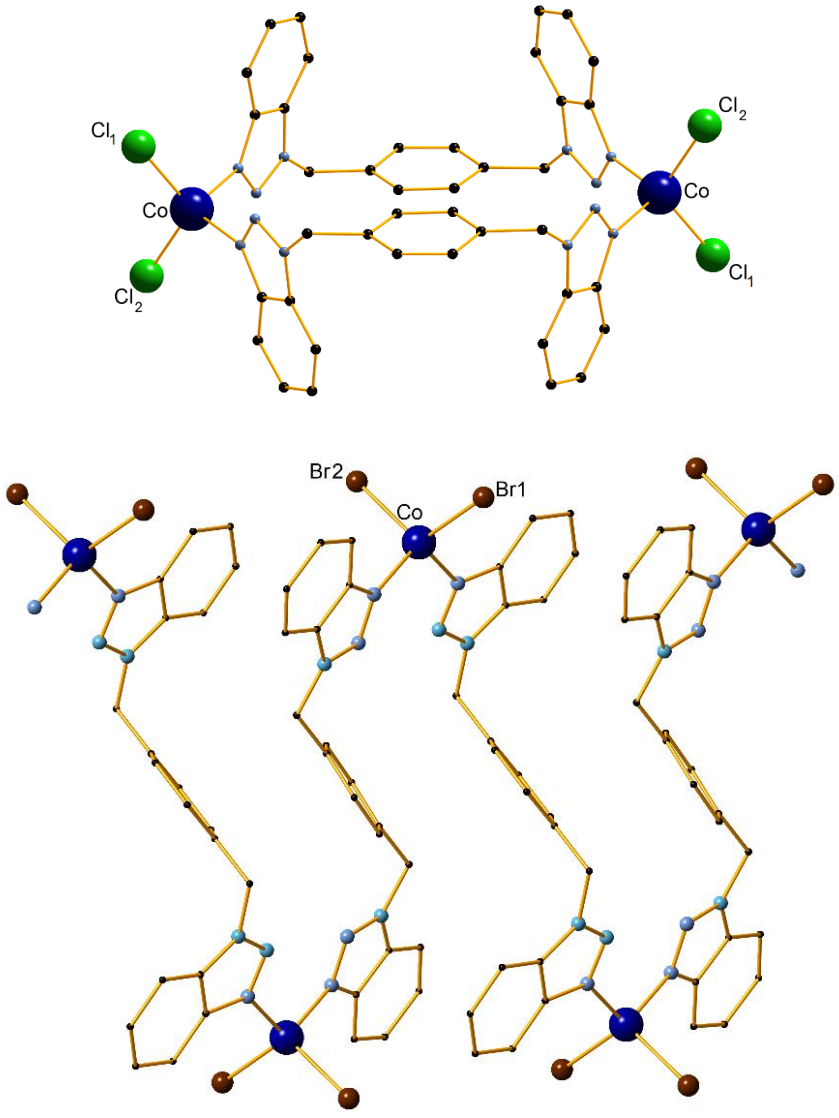

Figure 1. (upper) The structure of compound **1**. (lower) Part of the 1D framework of compound **2**. In each case the ligand adopts a different conformation (boat or chair). H atoms and solvent molecules are omitted for clarity. Color code Co (blue), Cl (green), Br (brown), C (black), N (light blue).

Compounds **3** and **5** are isostructural, therefore only the former will be described in detail. Compound **3** crystallizes in the triclinic $P\bar{1}$ space group and contains one molecule in the asymmetric unit, forming a zero-dimensional dimer structure (Figure 2). The unit consists of one Co^{II} center, one L^2 molecule, two chlorine atoms which act as terminal ligands and an acetonitrile molecule in the lattice. Co^{II} is coordinated to four atoms (Cl1, Cl2, N1, N6) and exhibits a slightly distorted tetrahedral geometry. The conformation (boat) and coordination sites of the ligand are detailed in Scheme 2 (Mode C). The mean Co-N distances are 2.0341(2) and 2.0352(2) Å respectively, while the Co-Cl distances were measured at 2.0352(17) and 2.0341(17) Å. Angles of the tetrahedron range from 100.470(8)° to 113.250(7)°. Co···Co distance was found to be 11.1122(11) Å. As in the case of compound **1**, the supramolecular architecture is further stabilized by the formation of inter-molecular π···π interactions (Figure S2), as described in Table S4. Again, no hydrogen bonds are formed.

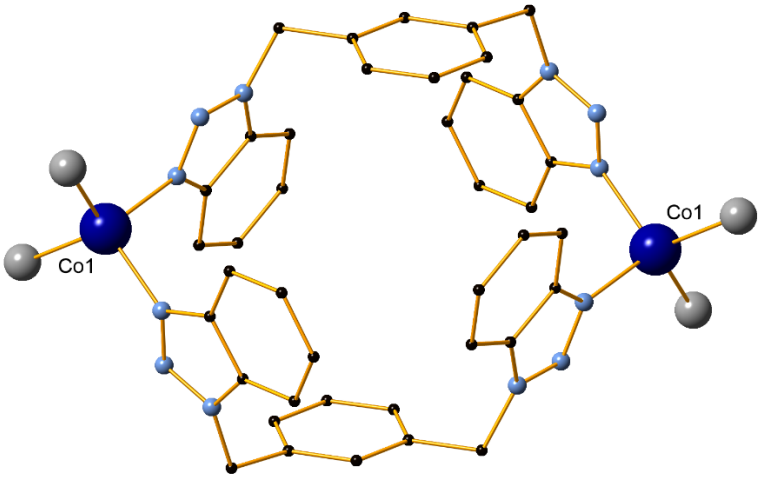

Figure 2. The structure of compounds **3** and **5**. X = Cl (**3**), Br (**5**). H atoms and solvent molecules are omitted for clarity. Color code Co (blue), X (grey), C (black), N (light blue).

Compound **4** crystallizes in the monoclinic space group $P2_1/c$ and contains one molecule in the asymmetric unit. The unit consists of one Co^{II} center, one L^2 molecule and two chlorine atoms. Co^{II} is coordinated to a total of five atoms and exhibits a distorted trigonal bipyramidal geometry ($\tau = 0.33$).[77]

The basal plane consists of one nitrogen atom from the ligand (N1) and the two chlorine atoms (Cl1 and Cl2), while the apical positions are occupied by a nitrogen and a chlorine atom from symmetry related molecules (N6 and Cl1). In contrast to compound **3**, which has the same molecular formula and its structure is zero-dimensional, the structure of **4** propagates in two directions through the formation of a chlorine bridge and the concurrent rotation of the non-rigid C-N bond (Figure 3, left / Scheme 2, Mode D). This results to the construction of a 2D framework, which consists of layers that are formed along the *b*0*c* plane axis (Figure 3, right). This packing arrangement allows for the formation of π···π inter-molecular interactions between certain benzotriazole aromatic rings, as detailed in Table S5. These weak interactions further facilitate to the stability of the framework (Figure S3). Considering each $Co^{II}_2Cl_2$ unit as a node the topological evaluation of **4** results in a uninodal 4-connected **sql** network with node distances at 11.724Å.

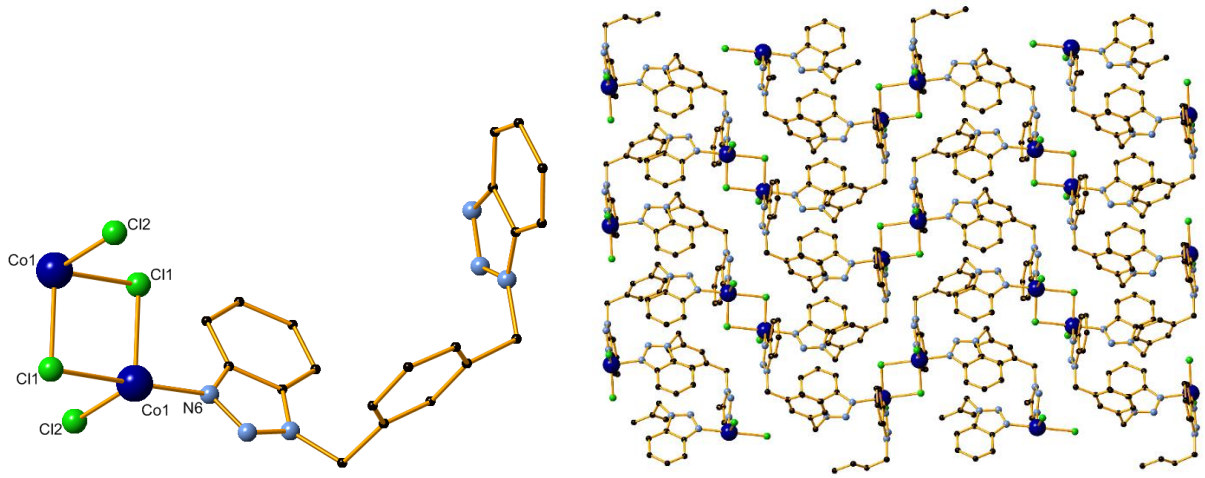

Figure 3. (left) The structure of compound **4**. H atoms are omitted for clarity. Color code Co (blue), Cl (green), C (black), N (light blue). (right) Part of the 2D framework of compound **4** along the *b*0*c* plane axis. H atoms are omitted for clarity.

Compound **6** crystallizes in the monoclinic space group $P2_1/c$. The unit consists of the Co^{II} center, one L^2 molecule, one lattice acetonitrile molecule and one nitrate which acts as a terminal ligand (Figure 4, upper). The geometry of Co^{II} is octahedral as it is coordinated to four nitrogen atoms from L^2 molecules

(N1, N1, N6, N6), which consist the basal plane and two nitrate oxygen atoms (O1, O1) which occupy the axial positions. The respective mean Co1-N1 and Co1-N6 distances are at 2.15789(10) and 2.19315(8) Å, the longest observed in this study. The Co-O1 distance was measured at 2.0920(13) Å. In this case, the ligand adopts a chair conformation (Scheme 2, Mode E) and as a result the structure extends to two dimensions along the *b*0*c* plane axis, forming a 2D coordination polymer (Figure 4, lower). No hydrogen bonds or other supramolecular interactions were observed. Considering each Co^{II} center as a node, the topological analysis of **6** results, as in the case of compound **4**, in a uninodal four-connected **sql** network with node distances at 12.908Å.

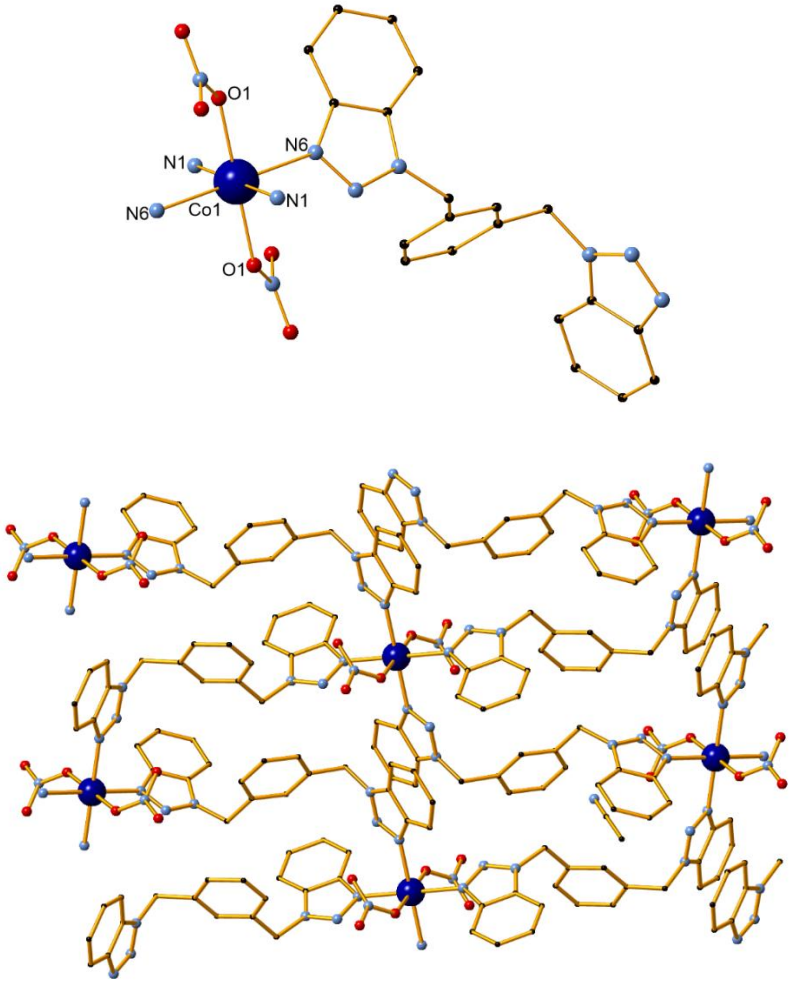

Figure 4. (upper) The structure of compound **6**. H atoms are omitted for clarity. Color code Co (blue), C (black), N (light blue), O (red). (lower) Part of the 2D architecture of compound **6** along the *b*0*c* plane axis. H atoms are omitted for clarity.

Compound **7** crystallizes in the monoclinic space group $P2_1/c$ and contains one molecule in the asymmetric unit. The unit consists of one Co^{II} center, one organic ligand molecule, two chlorine atoms and a lattice acetonitrile molecule. Co^{II} is coordinated to the two chlorine atoms (Cl1, Cl2) and to two nitrogen atoms (N1, N6), from the ligand molecule and a symmetry related ligand molecule respectively. The metal center therefore has a coordination number of four and exhibits a slightly distorted tetrahedral geometry, with the angles of the tetrahedron ranging from 105.402(10)° to 114.2428(14)°. The mean Co-N distance is 2.048(2) Å, and the Co-Cl distances are 2.2348(9) and 2.2254(9) Å. In this conformation of the ligand (Scheme 2, Mode F), the rotation of the non-rigid C-N bond brings the planes of the benzotriazole molecules to a 44.61(7)° angle. As a result, the structure propagates in one direction and unfolds in a helix-like manner, with the complex forming one dimensional (1D) chains (Figure 5).

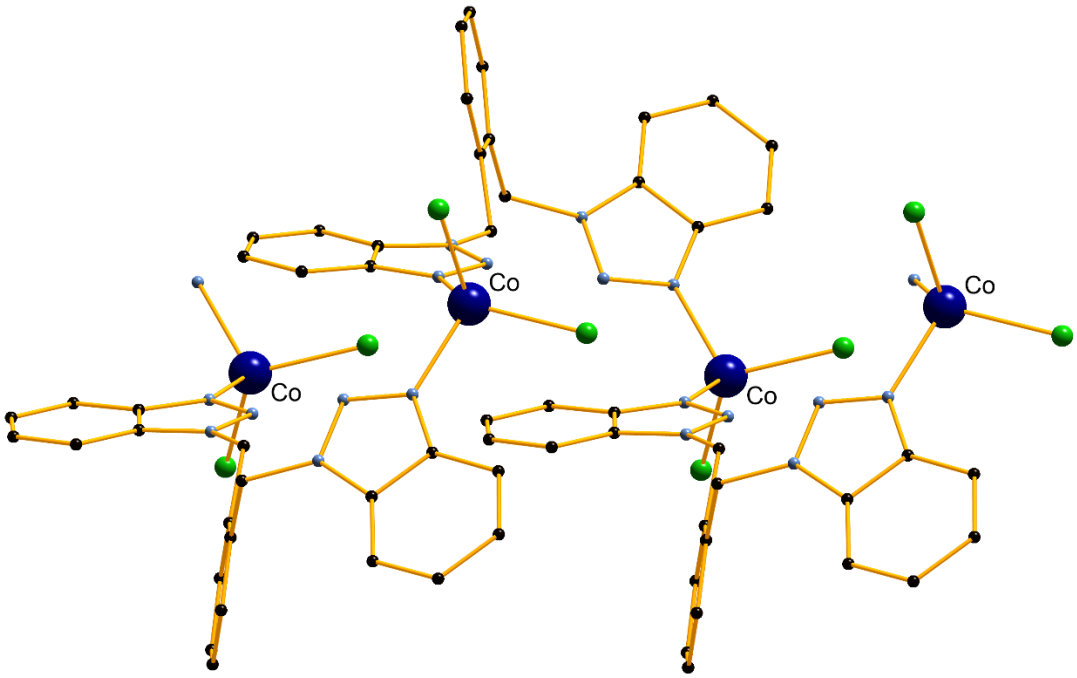

Figure 5. Part of the 1D framework of compound **7**. H atoms and solvent molecules are omitted for clarity. Color code Co (blue), Cl (green), C (black), N (light blue).

Compounds **8** and **9** are isostructural and as such only **8** will be described below. The compound crystallizes in the triclinic space group $P\bar{1}$ with one molecule in the asymmetric unit. The unit contains

one Co^{II} center, one L^3 molecule and two chlorine atoms which act as terminal ligands. Co^{II} is coordinated to four atoms in a N_2Cl_2 environment and exhibits a slightly distorted tetrahedral geometry. The mean Co-N distances are 2.041(3) and 2.032(3) Å, and the Co-Cl distances are 2.2350(13) and 2.2378(13) Å. Angles of the tetrahedron range from 104.32(14)° to 119.73(6)°. Co···Co distance was found to be 9.0147(19) Å. In this conformation of the ligand (Scheme 2, Mode G), the angle between the planes of the benzotriazole molecules is a 123.05(3)°. As the 1,2,3-triazole moieties are now in a different arrangement compared to **7**, compound **8** is eventually a zero-dimensional dimer structure (Figure 6). As in the previous dimers, inter-molecular π···π stacking interactions are formed to facilitate the stability of the supramolecular network (Figure S4, lower). Additionally, there is an intra-molecular π···π interaction within the dimer, formed between the aromatic rings of benzotriazole molecules (Figure S4, upper). Details for these interactions are listed in Table S6.

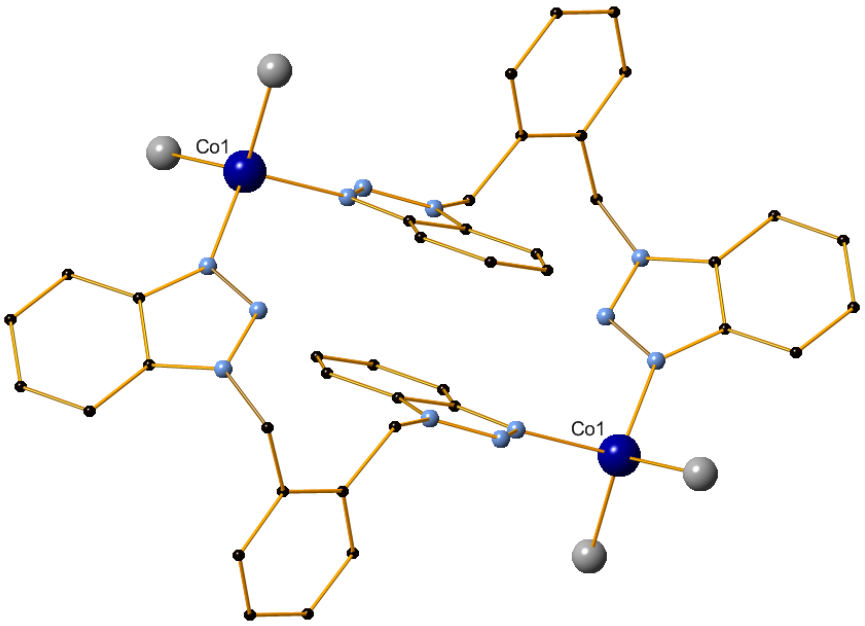

Figure 6. The structure of compounds **8** and **9**. X = Cl (**8**), Br (**9**). H atoms and solvent molecules are omitted for clarity. Color code Co (blue), X (grey), C (black), N (light blue).

Compound **10** crystallizes in the triclinic $P\bar{1}$ space group and contains one molecule in the asymmetric unit. The unit consists of one Co^{II} center, one organic ligand molecule, and a nitrate anion which acts as a terminal ligand. The metal center is coordinated to six atoms and exhibits a distorted octahedral geometry. Four nitrogen atoms from symmetry related ligand molecules (N3, N3, N6, N6) occupy the equatorial positions of the octahedron, while two nitrate oxygen atoms (O2, O2) occupy the axial positions. The Co-N and Co-O distances are 2.186(3) and 2.095(2) respectively. The coordination mode and conformation of the ligand in this case is similar to the zero-dimensional dimers **8** and **9** (Scheme 2, Mode G). However the octahedral geometry of Co^{II} in compound **10** means that the structure forms a neutral one-dimensional (1D) framework with small voids, which can be seen in Figure 7.

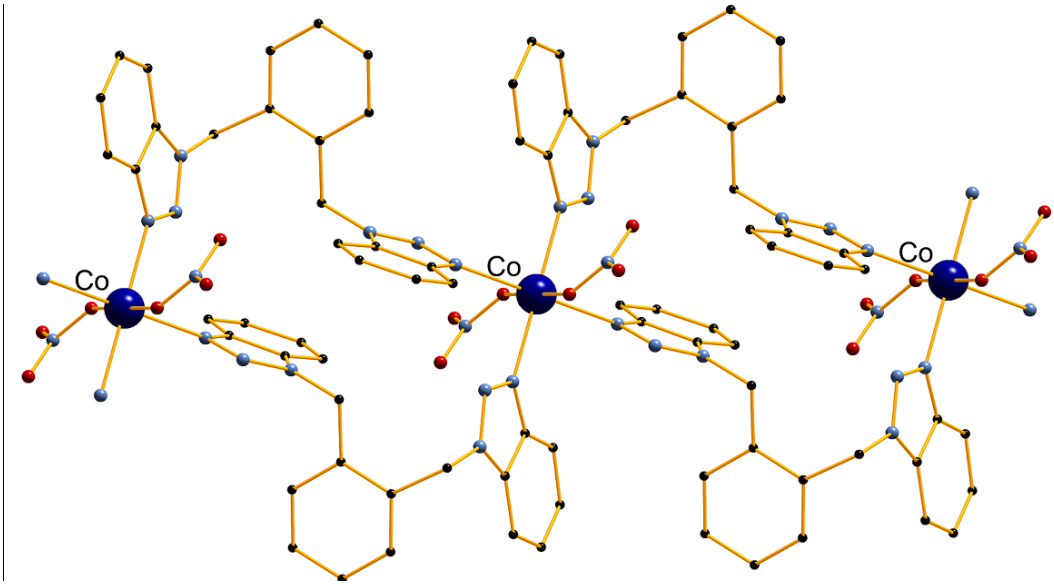

Figure 7. Part of the 1D framework of compound **10**. H atoms are omitted for clarity. Color code Co (blue), C (black), N (light blue), O (red).

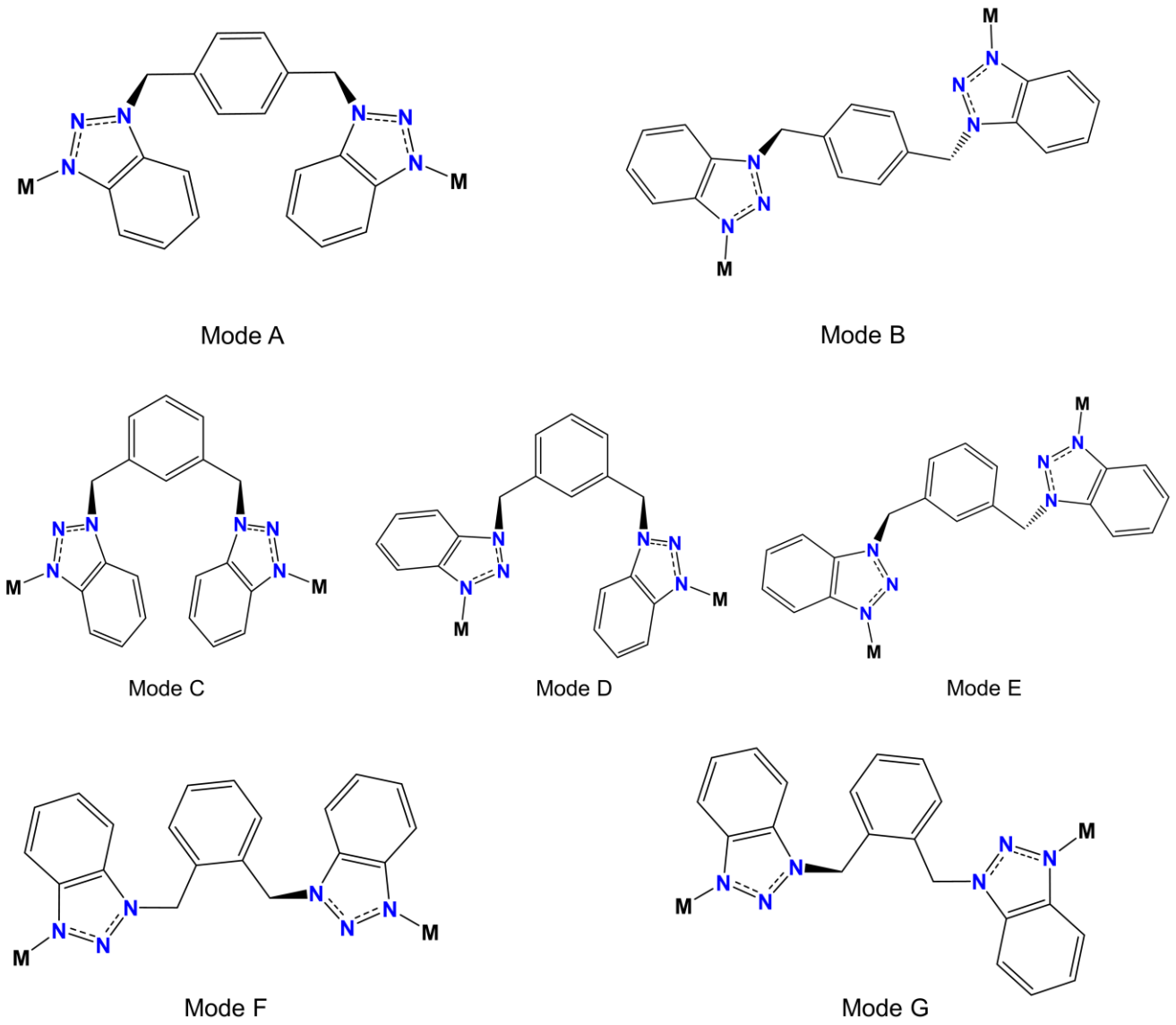

Scheme 2. The coordination modes of the ligands L^1 (upper, modes A, B), L^2 (middle, modes C-E), and L^3 (lower, mods F and G).

Table 1. Overview of the coordination characteristics of the compounds reported in this study.

Entry	Ligand	Compound	Geometry of Co^{II}	Coordination Mode	Dimensionality
1	L^1	**1**·2MeCN	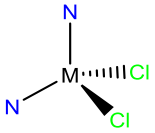	A	0D
2	L^1	**2**	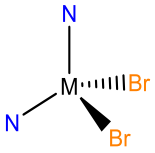	B	1D
3	L^2	**3**·MeCN	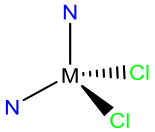	C	0D
4	L^2	**4**	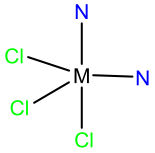	D	2D
5	L^2	**5**·2MeCN	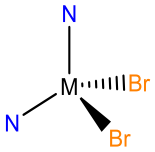	C	0D
6	L^2	**6**·2MeCN	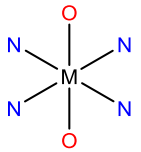	E	2D
7	L^3	**7**·2MeCN	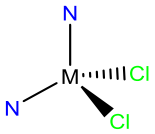	F	1D
8	L^3	**8**	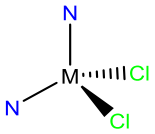	G	0D
9	L^3	**9**	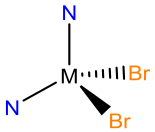	G	0D
10	L^3	**10**	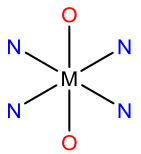	G	1D

Solution studies. Electrospray ionization mass spectrometry (ESI-MS) was also performed for compounds **1-10**, to confirm their identity in solution. The MS (positive-ion mode) for all complexes shows four peaks at the regions of 369.60, 539.65 and 709.75 and 880.32 m/z which perfectly correspond

to the respective $[Co(L)_2 - H]^{2+}$, $[Co(L)_3 - H]^{2+}$ and $[Co(L)_4 - H]^{2+}$ dicationic fragments. Additional peaks, depending on the anion present, are also observed. **1**, **3**, **4**, **7** and **8** show additional peaks at 434.04, 562.24, 774.18 m/z that correspond to the $[Co(L)Cl - H]^{1+}$, $[Co_2(L)Cl_3 - H]^{1+}$ and $[Co(L)_2Cl - H]^{1+}$ monocationic fragments respectively. Compounds **2**, **5** and **9** exhibit peaks at 479.95, 562.20, 696.75, 820.09, 1036.87 and 1160.24 m/z, corresponding to $[Co(L)Br - H]^{1+}$, $[Co(L)Br - H]^{1+}$, $[Co(L)Br_2 + 2H]^{1+}$, $[Co(L)_2Br - H]^{1+}$, $[Co_2(L)_2Br_3 - 3H]^{1+}$, and $[Co(L)_3Br - H]^{1+}$ fragments. For **6** and **10** two peaks appear at 461.06 and 801.20 m/z, that match the $[Co(L)(NO_3) - H]^{1+}$ and $[Co(L)_2(NO_3) - H]^{1+}$ monocationic fragments respectively. Due to the similar behavior of all compounds, representative ESI-MS spectra are presented in Figure S11.

TGA - PXRD studies. Thermogravimetric analysis (TGA) between room temperature and 900-1000 °C was carried out on all compounds (Supporting Information, Figures S12-S14). All compounds start to decompose in the region of 200-350°C. In compounds with lattice solvent molecules, this loss takes place in the region of 70-190 °C. To confirm phase purity of the samples, representative compounds **7**, **8** and **9** were further characterized through Powder XRD studies, indicating that they are indeed formed in high purity (Figures S8-S10).

Synthetic aspects. As shown in Table 1, the employment of L^1, L^2 and L^3 along with Co^{II} sources afforded a variety of compounds, including 0D dimers and 1D or 2D CPs. This structural diversity is owed to the ligand, ratio, temperature and metal source used. As such, these parameters and their importance to this study will be further discussed below. While various solvents were tested during synthesis, only acetonitrile and acetone were successful. The choice of solvent, however, does not seem to play any significant part in the resulting compounds and therefore will not be discussed in further detail.

A close inspection of the ratio and temperature conditions used provides a significant understanding of the system and allows for its finer control. In regards to the ratio, the complexes **1**-**5**, **7**, **9** and **10** were synthesized using either a 1:1 or a 2:1 metal-ligand ratio. Interestingly, other ratios were

not so successful, resulting mostly in non-crystalline material. The only exceptions to this were **1** and **7**, which were also prepared in a 1:2 ratio, and **6** and **8** which were synthesized in a 3:1 ratio. None of the ten compounds could be afforded in larger ratios.

Introduction of the temperature parameter through various forms (gentle heating to 50°C, solvothermal reactions to 75-100°C) led to more interesting results. In several cases, an increase in temperature during synthesis allowed for a better control of the resulting product through manipulation of the non-rigid part of the ligands. In the L^1-based compounds **1** and **2**, the former was synthesized in room temperature (rt), while the latter was prepared under 50°C. This temperature effect has a subsequent result in the conformation of the ligand (Scheme 2, Modes A and B) which allows for the manipulation of the dimensionality in the structures; **1** is a 0D dimer while **2** is a 1D coordination polymer. Another interesting example is observed in the L^2-based compounds **3** and **4**. Both were prepared in the same method, however **3** was synthesized in rt and produced a 0D dimer, while **4** was subjected to 75°C heating and afforded a 2D coordination polymer. A closer comparison of the structures reveals a rotation of the non-rigid C-N bond in L^2, which can be attributed to the temperature effect in each case. To investigate this further, single crystals of **3** were heated to 75°C for 18 hours, and after X-Ray crystallography analysis were found to have been converted to compound **4**, confirmed also by IR spectra. Thus, compound **3** can undergo a temperature-induced single crystal transformation to **4** (Scheme 3), subjecting to significant alterations: the coordination geometry of Co^{II} changes from tetrahedral to trigonal bipyramidal, the dimensionality of the structure changes from 0D to 2D, and the loss of lattice solvent is also observed. In regards to the crystallographic parameters, there are considerable differences in the space group ($P\bar{1}$ to $P2_1/c$) and unit cell dimensions. Efforts to make this transformation reversible were unsuccessful.

Taking our findings up to this point into consideration, we envisioned that a combination of higher temperatures and large metal:ligand ratios would allow for further structural variety. Indeed,

compounds **6** and **8** were synthesized employing a 3:1 ratio and solvothermal reaction. As evident by a comparison of **8** to **7** (synthesized in rt), temperature once again affects the conformation of the ligand's non-rigid part, leading to a 0D dimer and a 1D chain respectively. Efforts to obtain **6** and **8** using different ratios or in the absence of high temperature proved unsuccessful, indicating the importance of both parameters in controlling the system.

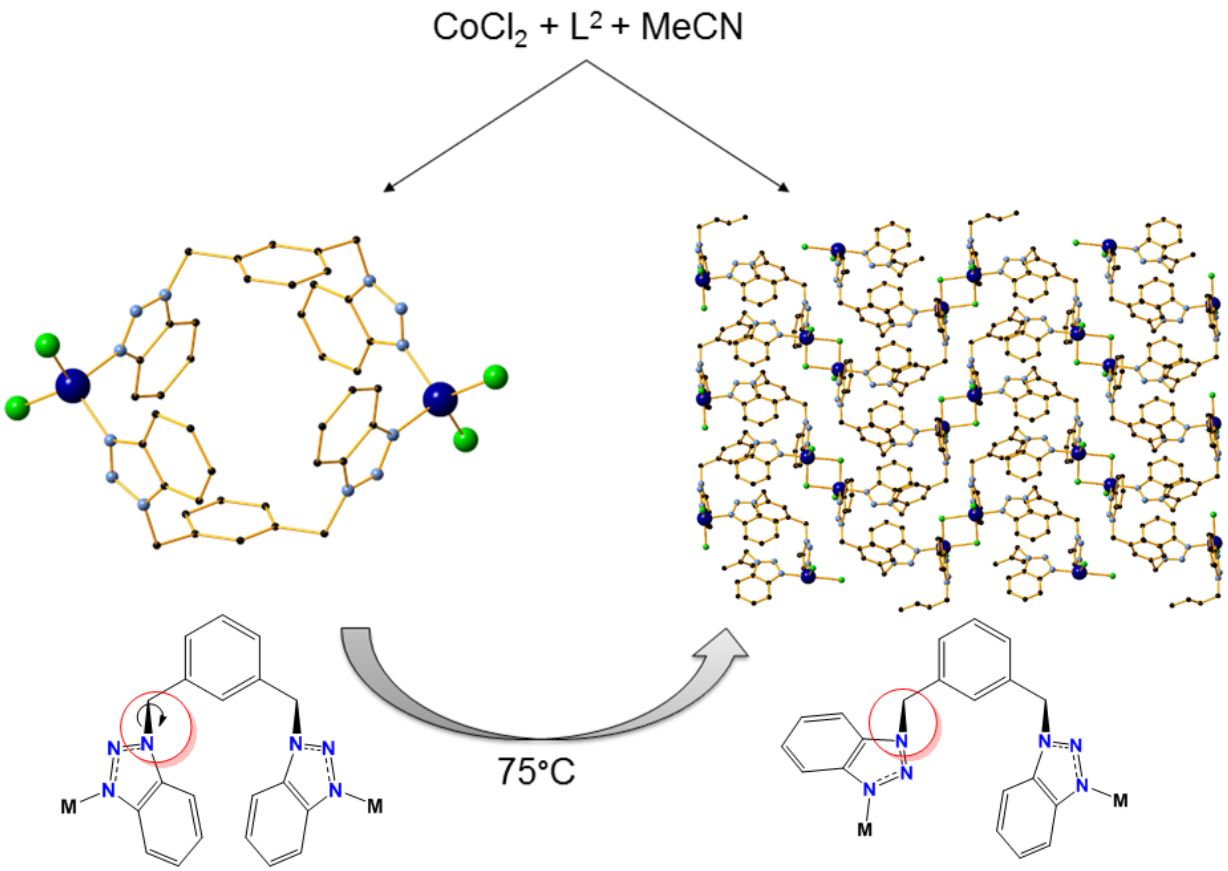

Scheme 3. A schematic representation of the temperature-induced single-crystal to single-crystal transformation of **3** to **4.**

A classification of complexes **1**-**10** by ligand reveals that the para-substituted ligand L^1 afforded the lowest number of structures, as only a 0D dimer and a 1D CP were obtained from this ligand. In contrast, four complexes were synthesized using each of the meta- and ortho-substituted ligands L^2 and L^3 respectively; two 0D dimers and two multi-dimensional CPs in each case. In all complexes,

coordination of the Co^{II} center takes place only through the far N atom of the 1,2,3-triazole moiety; coordination through the N-2 atom is likely prevented by steric effects. L^1, L^2 and L^3 also contribute to the stability of the respective 0D dimers via participation to intermolecular $\pi\cdots\pi$ stacking interactions. The present findings, summarized in Table 1, recommend that ligand L^2, with substitution in meta position, is more appropriate for the synthesis of porous 2D materials, while L^1 and L^3 are suitable for the construction of cage like or one dimensional polymeric structures. The coordination chemistry of this family of organic ligands has received less attention, whereas the corresponding benzimidazole derivatives have been extensively used, along with polycarboxylate ligands, for the synthesis of 2D or 3D porous materials.

In regards to the cobalt sources, a variety of sources were used in order to perform a full systematic study for the metal, including $CoCl_2$, $CoBr_2$, $Co(NO_3)_2$, $Co(OAc)_2$, $Co(BF_4)_2$, $Co(ClO_4)_2$ and $Co(SO_4)_2$. Out of these salts, only the first three afforded any results. Interestingly, each anion appears to contribute differently to the dimensionality of the structures. Cl plays a significant role in compound **4**, as the structure propagates in two directions through the formation of a chlorine bridge. Bromine-based complexes have less frequency and variation, despite our efforts to produce results similar to the chloride-based structures. Finally, experiments with Co^{II} nitrate lead exclusively to coordination polymers, as compounds **6** and **10** are 1D and 2D respectively. This change in anion is also accompanied by a drastic change in the geometry of the metal center, as all nitrate-based compounds exhibit octahedral Co^{II} centers.

Magnetic, Spectroscopic and Theoretical Studies. We have investigated a selection of complexes, **4**, **7** and **9**, with SQUID magnetometry, Electron Paramagnetic Resonance (EPR) spectroscopy and *ab initio* Complete Active Space Self-Consistent Field Spin-Orbit (CASSCF-SO) calculations to elucidate their magnetic properties. Complexes **7** and **9** contain Co(II) in a distorted tetrahedral environment, while the Co(II) site in **4** is a distorted trigonal bipyramid, giving in all cases an anisotropic $S = 3/2$ ground state. Complex **7** is a 1D CP, the nearest-neighbour Co-Co distance is over 8.5 Å and the through-bond

connectivity involves 10 ligand N and C atoms, thus we treat the Co sites as uncoupled. Complex **9** is a discrete 0D dimeric species with intramolecular π-π stacking, thus some magnetic interaction between the two Co(II) ions may be present. Complex **4** is a 2D CP featuring a repeat unit of a μ_2-Cl^- bridged dimer and thus it is expected that the magnetic interactions between the Co^{II} ions in could be rather strong. Importantly, for both **4** and **9**, the Co ions are related by crystallographic inversion symmetry and hence must have the same local electronic structure. We begin by investigating **7**, followed by **9** and **4**, following the expected level of complexity.

The magnetic susceptibility-temperature product, $\chi_M T$, for **7** has a value of 2.71 cm^3 mol^{-1} K at room temperature and is more-or-less temperature independent until it begins to fall below 30 K to reach a minimum value of 1.67 cm^3 mol^{-1} K at 2 K (Figure 8). The isothermal magnetization, *M*, profiles at 2 and 4 K approach and the same maximum value, but fail to saturate at 7 T with values of 2.78 and 2.73 μ_B mol^{-1} and are non-superimposible on a reduced magnetization plot, (Figure S5). The low temperature drop in $\chi_M T$, the lack of saturation of *M* and the non-superimposable reduced *M* plots all suggest significant Zero-Field Splitting (ZFS) of the ground $S = {}^3/_2$ state in this isolated tetrahedral Co^{II} species. The ZFS was estimated by fitting these magnetic data simultaneously with the PHI program,[78] using the spin Hamiltonian in Equation 1. With the *E* term fixed to zero to avoid over parameterization, reasonable fits are obtained for $D \approx \pm 7$ cm^{-1} and $g \approx 2.3$. The cryogenic X- and Q-band (ca. 9.4 and 34 GHz, respectively) EPR spectra for compound **7** show a reasonably broad feature around 0.15 and 0.45 T, respectively (Figure 9). We find that the relative intensity of the two features in the Q-band spectrum can only be reproduced when $D \approx -7$ cm^{-1}; subsequent optimization of the parameters against the magnetometry and EPR data yields $D = -6.53$ cm^{-1}, $E = 0.379$ cm^{-1} and $g = 2.26$, with frequency-space Lorentzian linewidths of η(X-band) = 3 GHz and η(Q-band) = 6 GHz. Introducing further flexibility to the Hamiltonian with anisotropic *g*-values and/or anisotropic linewidths does not improve the simulation; furthermore, it is likely that hyperfine coupling of the electron spin to the 100% naturally abundant ^{59}Co nucleus with $I = {}^7/_2$ is responsible for these strange line shapes. Indeed, CASSCF-SO calculations on the

Co-containing repeat unit of **7** confirm our experimental findings, suggesting D = -8.3 cm^{-1}, E = 1.0 cm^{-1} and g = 2.31.

$$\hat{H}_1 = D\left(\hat{S}_z{}^2 - \frac{1}{3}\hat{S}^2\right) + E(\hat{S}_+{}^2 + \hat{S}_-{}^2) + g\mu_B\hat{S}\cdot B \quad (1)$$

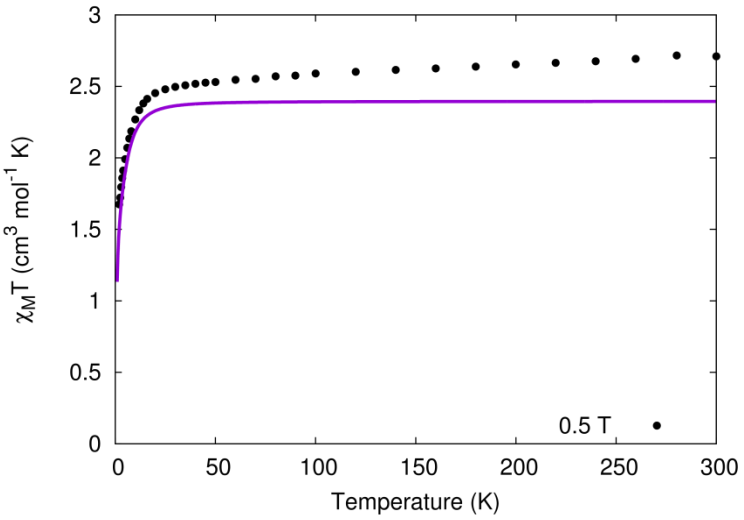

Figure 8. Experimental (black circles) and fitted (purple line, parameters in text) $\chi_M T$ for **7** in a 0.5 T field.

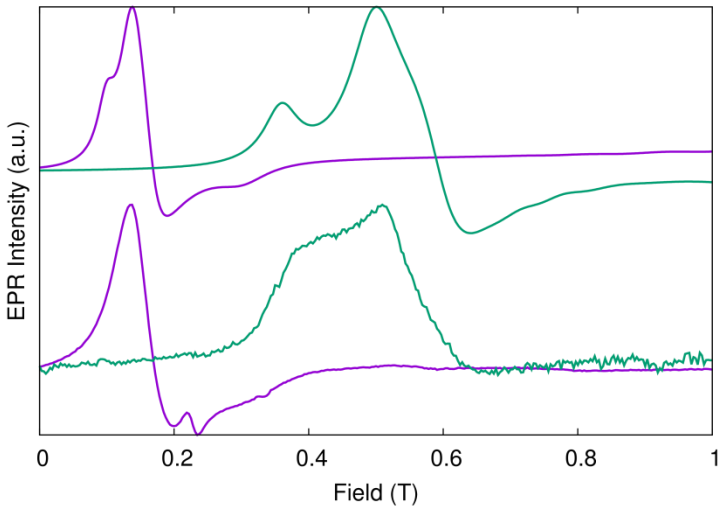

Figure 9. Experimental (lower traces) and simulated (upper traces, parameters in text) EPR spectra for a polycrystalline powder of **7** at 9.39557 GHz (purple) and 34.049 GHz (green) at 5 K. Note that the feature at ~ 0.23 T in the X-band spectrum is a background signal

The $\chi_M T(T)$ for **9** has value of 5.55 $cm^3\ mol^{-1}$ K (per dimer) at room temperature that is roughly constant until it declines below 40 K to reach 1.15 $cm^3\ mol^{-1}$ K at 2 K (Figure 10). While the $\chi_M T(T)$ is broadly similar in profile to that of **7**, the magnetization data at 2 and 4 K show quite different behavior compared with **7**, where the two isotherms are coincident until ca. 1 T where they separate before approaching one another again at 7 T reaching 4.39 and 4.25 $\mu_B\ mol^{-1}$, respectively (Figure 10, inset). It is impossible to reproduce this data using the spin Hamiltonian Equation 1 for each site of the dimer, as the strange sigmoidal shape of the magnetization data is directly indicative of antiferromagnetic interactions. Thus, we begin by modelling the magnetic data using the spin Hamiltonian Equation 2 which takes into account an isotropic interaction between the two Co^{II} ions. Using the same initial minimal model as previously with *E* fixed to zero, we fit the magnetic data to find two minima: D = -19.9 cm^{-1}, g = 2.38, J = -0.319 cm^{-1}, and D = 26.8 cm^{-1}, g = 2.41, J = -0.559 cm^{-1}. EPR spectra for **9** at X- and Q-band show only one broad resonance at each frequency (Figure 11). Of the two parameter sets determined from the magnetic data, only the $D < 0$ set is in agreement with the EPR data. Further refinement of these parameters gives D = -19.6 cm^{-1}, g = 2.38, J = -0.319 cm^{-1} with frequency-space Lorentzian linewidths of η(X-band) = 6 GHz and η(Q-band) = 12 GHz. Given the lack of fine structure in the EPR spectra, it is not possible to further refine the model to estimate the rhombicity of the local ZFS tensors. *Ab initio* CASSCF-SO calculations on single sites of **9** again lend support to our conclusions, predicting D = -12.3 cm^{-1}, E = 2.6 cm^{-1} and g = 2.34; furthermore the trend of D for **9** being greater than for **7** is also verified.

$$\widehat{H}_2 = \sum_{i=1}^{2}[D\left(\hat{S}_{i,z}{}^2 - \frac{1}{3}\hat{S}_i{}^2\right) + E(\hat{S}_{i,+}{}^2 + \hat{S}_{i,-}{}^2) + g\hat{S}_i \cdot B] - 2J\hat{S}_1 \cdot \hat{S}_2 \qquad (2)$$

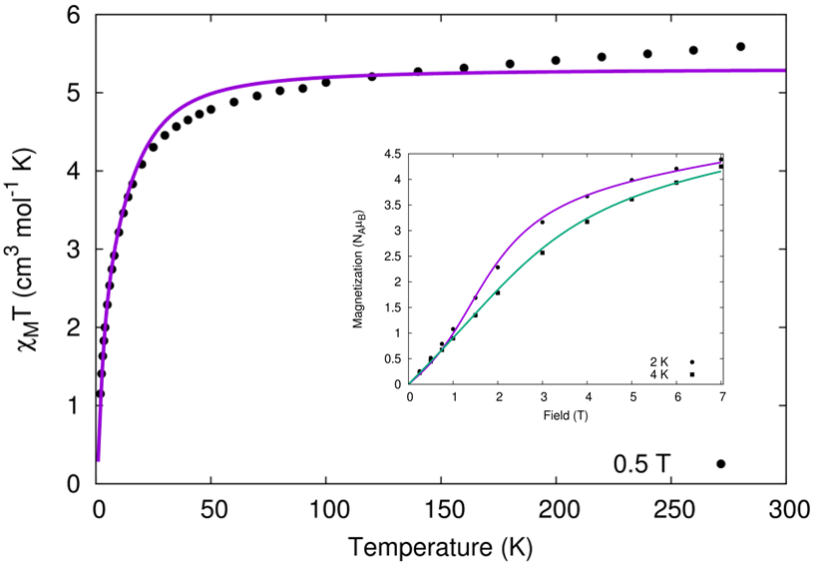

Figure 10. Experimental (black circles) and fitted (purple line) $\chi_M T$ for **9** in a 0.5 T field. (inset) Experimental (black circles and squares) and fitted (purple and green lines) magnetization for **9** at 2 and 4 K.

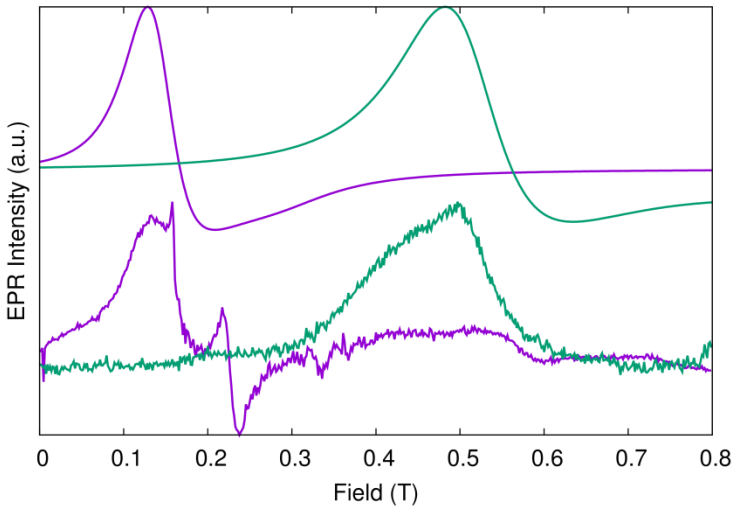

Figure 11. Experimental (lower traces) and simulated (upper traces, parameters in text) EPR spectra for a polycrystalline powder of **9** at 9.40040 GHz (purple) and 33.927 GHz (green) at 5 K. Note that the feature at ~ 0.23 in the X-band spectrum is a background signal

$\chi_M T$ vs. T for compound **4** is similarly temperature independent from 300 K down to 20 K, with a value of 6.04 $cm^3\ mol^{-1}$ K at 300 K, before a small increase to a maximum value of 6.22 $cm^3\ mol^{-1}$ K at 7 K followed by falling to reach 4.95 $cm^3\ mol^{-1}$ K at 2 K (Figure 12). Such a rise directly indicates exchange coupling between the Co(II) ions. The magnetization vs. field data at 2 and 4 K and 7 T are nearly coincident with a value of 5.35 $\mu_B\ mol^{-1}$, indicating a well isolated ground manifold (Figure 12, inset). Owing to the likely presence of significant magnetic exchange in this case and given that our CASSCF-SO calculations have been good estimates for **7** and **9**, we propose to use such calculations for **4** in order to estimate the local electronic structure of the Co^{II} centers. As the Co sites are related by crystallographic inversion symmetry, both will possess the same local electronic structure; the calculations suggest that the Co^{II} ions are subject to a very large ZFS of D = +48.4 cm^{-1} with E = -8.9 cm^{-1} and g = 2.38 (note that the sign of D is also different to **7** and **9**). The very large ZFS leads to a well-isolated ground Kramers doublet (first excited state at ~ 114 cm^{-1}) with effective g-values of g_1 = 1.8, g_2 = 3.5 and g_3 = 6.5 that are approximately associated with metal-ligand directions in the first coordination sphere; g_1 is associated with the approximate three-fold axis of the trigonal bipyramid (Cl1-Co1-N6), g_2 is associated with the other bridging Cl^- anion (Cl1'-Co1), and g_3 is perpendicular to the Cl1'-Co1-Cl1 plane (roughly along the Co1-N1 direction). Based on the prediction of a very large ZFS with $D > 0$, the magnetic data for **4** can be satisfactorily modelled using Equation 2 with D = +10 cm^{-1}, E = -2 cm^{-1}, g = 2.5 and J = +1 cm^{-1}. This model gives effective g-values for the ground Kramers doublet of each Co^{II} ion as g_1 = 2.2, g_2 = 3.4 and g_3 = 6.3, which are in excellent agreement with those suggested by CASSCF-SO calculations. The characteristic rise in $\chi_M T$ at the lowest temperatures can loosely be associated with a ferromagnetic interaction, however this is a poor description when the local ZFS >> J. EPR spectra for **4** are much more featured than for **7** and **9**, and show a general decrease in intensity on increasing temperature, Figures 18 and 19. The X-band spectra show a structured resonance at low field, while the Q-band spectra show four clear resonances from 0.16 to 1.2 T. Owing to the large ZFS and small exchange interaction, the EPR experiments only probe the four lowest lying states of the exchange coupled manifold. Therefore,

the most appropriate model for these data is the pseudo-spin S = 1/2 model, where the lowest lying Kramers doublet of each Co^{II} ion is treated as a S = 1/2 state with the magnetic anisotropy given by three principal g-values, and the intramolecular interaction modelled with an anisotropic effective exchange term, Hamiltonian Equation 3. Fixing the local orientations of the g-tensors from the CASSCF-SO calculations, and approximating the Cl1'-Co1-Cl1 angle as 90° (it is 84.5° from X-Ray crystallography), the local $\overline{\overline{g_e}}$ matrix of each site is rotated around the z-axis by ±45° and thus the model is constructed according to Figure 15. The anisotropic exchange term is approximated by considering a unique value for J_x connecting the Co^{II} ions with fixed $J_y = J_z$. The best simulation was obtained with g_1 = 1.84, g_2 = 3.61, g_3 = 5.36, J_x = ±0.240 cm^{-1} and J_{yz} = ±0.344 cm^{-1} with anisotropic frequency-space Lorentzian linewidths of η_{xy}(X-band) = 3 GHz, η_z(X-band) = 5 GHz, η_{xz}(Q-band) = 5 GHz and η_y(Q-band) = 10 GHz (Figures 13 and 14), which is in good agreement with the effective g-values determined both by CASSCF-SO and the magnetometry data. We note that the spectra are insensitive to the overall sign of the J terms, however the relative signs of both must be the same (i.e. the product J_xJ_{yz} is positive). While this model is unable to replicate the magnetometry data directly owing to the influence of excited states, simulation of $\chi_M T$ for J_x and J_{yz} positive shows an increase at the lowest temperatures, compared to a decrease with J_x and J_{yz} negative (Figure S7) and hence we suggest that J_x and J_{yz} are both positive.

$$\hat{H}_3 = \mu_B(\hat{S}_1 \cdot \overline{\overline{g_e}} + \hat{S}_2 \cdot \overline{\overline{g_e'}}) \cdot B - 2(J_x \hat{S}_{1,x}\hat{S}_{2,x} + J_{yz}(\hat{S}_{1,y}\hat{S}_{2,y} + \hat{S}_{1,z}\hat{S}_{2,z})) \quad (3)$$

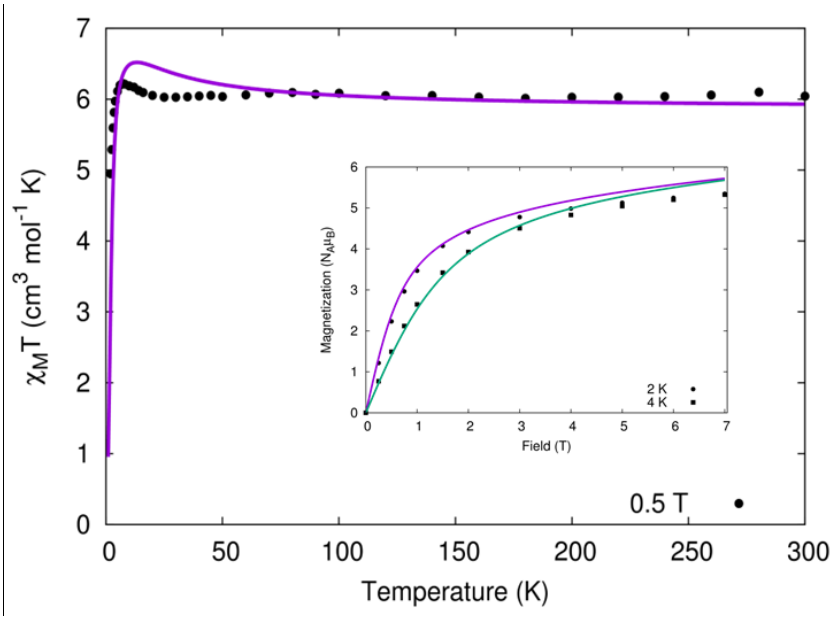

Figure 12. Experimental (black circles) and simulated (purple line) $\chi_M T$ for **4** in a 0.5 T field. (inset) Experimental (black circles and squares) and fitted (purple and green lines) magnetization for **4** at 2 and 4 K.

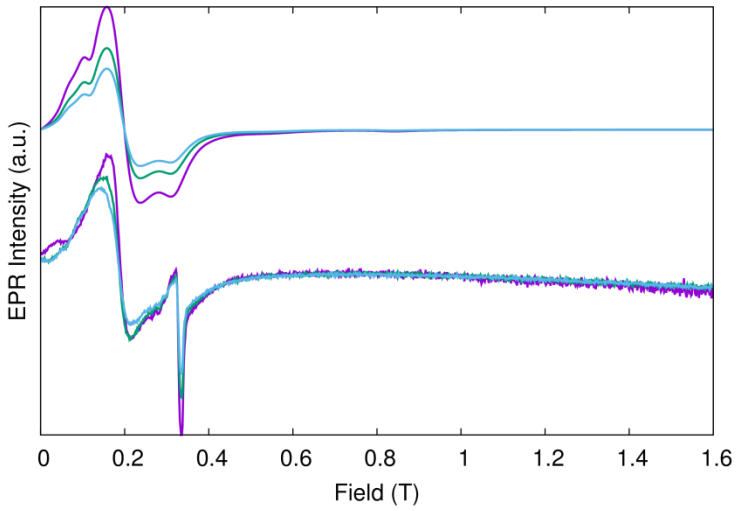

Figure 13. Experimental (lower traces) and simulated (upper traces) X-band EPR spectra for **4** at 9.3854 GHz and 5 (purple), 7.5 (green) and 10 (blue) K. Note that the feature at ~ 0.32 T is a background signal

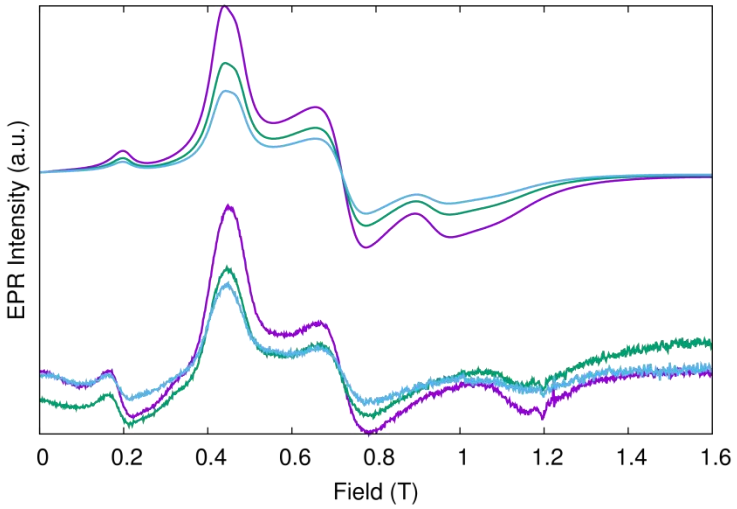

Figure 14. Experimental (lower traces) and simulated (upper traces) Q-band EPR spectra for **4** at 33.95 GHz and 5 (purple), 7.5 (green) and 10 (blue) K.

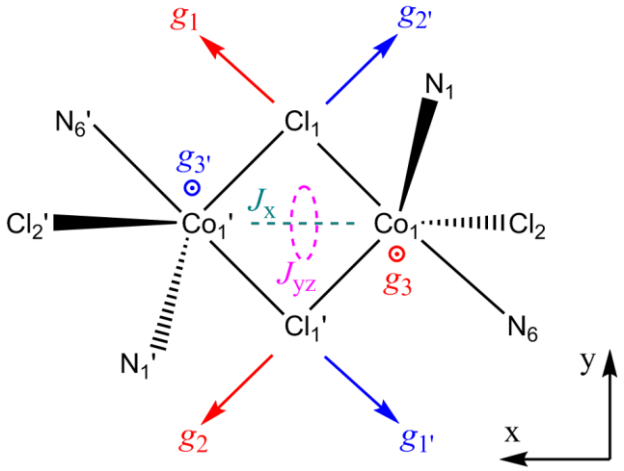

Figure 15. Relative orientations of principal *g*-values and exchange coupling terms in Hamiltonian Equation 3 for compound **4**.

CONCLUSION

In this work we studied the potential versatility of a series of benzotriazole-based semi-rigid ligands in cobalt coordination chemistry. The ten compounds derived from this systematic study reveal a large structural variety depending on synthetic parameters (ratio, temperature and salt) and flexible ligand

selection (various conformations in each ligand dependent on temperature). Tuning of these parameters allows for a greater control and manipulation of the system towards compounds with desired characteristics, resulting in a range of 0D dimers to 1D and 2D CPs with various metal geometries. A temperature-induced single-crystal to single-crystal transformation of compound **3** to **4** is additionally reported. The magnetic properties of a selection of representative compounds are subject to large changes with only minor structural variations, suggesting that tetrahedral Co^{II} nodes in CPs or MOFs could function as sensitive reporters of small changes in the local environment. Our future efforts will be dedicated to i) further exploiting such systems to synthesize 3D porous CP/MOFs, ii) investigating catalytic properties of these compounds, and iii) employing different metals to fully explore the coordination potential of the ligands.

ASSOCIATED CONTENT

Supporting Information. X-ray crystallographic files in CIF format for structures 1−10.

AUTHOR INFORMATION

Corresponding Author

* e-mail: G.Kostakis@sussex.ac.uk

Acknowledgments

We thank the EPSRC UK National Crystallography Service at the University of Southampton for the collection of crystallographic data for compound **2**.[69] The EPSRC UK National Electron Paramagnetic Resonance Service at The University of Manchester is also gratefully acknowledged. NFC thanks the Ramsay Memorial Trust for a Research Fellowship. We also thank Prof. David Collison for helpful discussions.

References

(1) Sun, L.; Campbell, M. G.; Dinca, M. *Angew. Chem. Int. Ed.* **2016**, *55*, 3566–3579.

(2) Thacker, N. C.; Lin, Z.; Zhang, T.; Gilhula, J. C.; Abney, C. W.; Lin, W. *J. Am. Chem. Soc.* **2016**, *138*, 3501–3509.

(3) Zeng, M. H.; Yin, Z.; Tan, Y. X.; Zhang, W. X.; He, Y. P.; Kurmoo, M. *J. Am. Chem. Soc.* **2014**, *136*, 4680–4688.

(4) Yan, Y.; Juríček, M.; Coudert, F.-X.; Vermeulen, N. A.; Grunder, S.; Dailly, A.; Lewis, W.; Blake, A. J.; Stoddart, J. F.; Schröder, M. *J. Am. Chem. Soc.* **2016**, *138*, 3371–3381.

(5) Liu, D.; Lu, K.; Poon, C.; Lin, W. *Inorg. Chem.* **2014**, *53*, 1916–1924.

(6) Cui, Y.; Chen, B.; Qian, G. *Coord. Chem. Rev.* **2014**, *273–274*, 76–86.

(7) Liu, X.; Cen, P.; Li, H.; Ke, H.; Zhang, S.; Wei, Q.; Xie, G.; Chen, S.; Gao, S. *Inorg. Chem.* **2014**, *53*, 8088–8097.

(8) Ma, T.; Li, M. X.; Wang, Z. X.; Zhang, J. C.; Shao, M.; He, X. *Cryst. Growth Des.* **2014**, *14*, 4155–4165.

(9) Liu, B.; Wei, L.; Li, N.-N.; Wu, W.-P.; Miao, H.; Wang, Y.-Y.; Shi, Q.-Z. *Cryst. Growth Des.* **2014**, *14*, 1110–1127.

(10) Desiraju, G. R. *J. Am. Chem. Soc.* **2013**, *135*, 9952–9967.

(11) Thalladi, V. R.; Goud, B. S.; Hoy, V. J.; Allen, F. H.; Howard, J. A. K.; Desiraju, G. R. *Chem. Commun.* **1996**, 401.

(12) du Plessis, M.; Barbour, L. J. *Dalton Trans.* **2012**, *41*, 3895–3898.

(13) Lin, Z.-J.; Lü, J.; Hong, M.; Cao, R. *Chem. Soc. Rev.* **2014**, *43*, 5867–5895.

(14) Furukawa, H.; Müller, U.; Yaghi, O. M. *Angew. Chem. Int. Ed.* **2015**, *54*, 3417–3430.

(15) Wilmer, C. E.; Leaf, M.; Lee, C. Y.; Farha, O. K.; Hauser, B. G.; Hupp, J. T.; Snurr, R. Q. *Nat. Chem.* **2012**, *4*, 83–89.

(16) Kostakis, G. E.; Malandrinos, G.; Nordlander, E.; Haukka, M.; Plakatouras, J. C. *Polyhedron* **2009**, *28*, 3227–3234.

(17) Liu, X.-G.; Wang, L.-Y.; Zhu, X.; Li, B.-L.; Zhang, Y. *Cryst. Growth Des.* **2009**, *9*, 3997–4005.

(18) Manna, B.; Desai, A. V.; Kumar, N.; Karmakar, A.; Ghosh, S. K. *CrystEngComm* **2015**, DOI: 10.1039/C5CE00139K.

(19) Burneo, I.; Stylianou, K.; Imaz, I.; Maspoch, D. *Chem. Commun.* **2014**, *50*, 13829–13832.

(20) Joarder, B.; Desai, A. V; Samanta, P.; Mukherjee, S.; Ghosh, S. K. *Chem. Eur. J.* **2015**, *21*, 965–969.

(21) Guo, J.-S.; Xu, G.; Jiang, X.-M.; Zhang, M.-J.; Liu, B.-W.; Guo, G.-C. *Inorg. Chem.* **2014**, *53*, 4278–4280.

(22) Manna, B.; Desai, A. V.; Ghosh, S. K. *Dalt. Trans.* **2016**, *45*, 4060–4072.

(23) Maji, T. K.; Matsuda, R.; Kitagawa, S. *Nat. Mater.* **2007**, *6*, 142–148.

(24) Yang, J.-X.; Qin, Y.-Y.; Cheng, J.-K.; Zhang, X.; Yao, Y.-G. *Cryst. Growth Des.* **2015**, *15*, 2223–2234.

(25) Ghosh, S. K.; Kitagawa, S. *CrystEngComm* **2008**, *10*, 1739.

(26) Tian, H.; Liu, R.; Wang, X.; Yang, P.; Li, Z.; Li, L.; Liao, D. *Eur. J. Inorg. Chem.* **2009**, 4498–4502.

(27) Dokorou, V. N.; Milios, C. J.; Tsipis, A. C.; Haukka, M.; Weidler, P. G.; Powell, A. K.; Kostakis, G. E. *Dalton Trans.* **2012**, *41*, 12501–12513.

(28) Bikas, R.; Hosseini-Monfared, H.; Vasylyeva, V.; Sanchiz, J.; Alonso, J.; Barandiaran, J. M.; Janiak, C. *Dalton Trans.* **2014**, *43*, 11925–11935.

(29) Henninger, S. K.; Habib, H. A.; Janiak, C. *J. Am. Chem. Soc.* **2009**, *131*, 2776–2777.

(30) Chaudhari, A. K.; Joarder, B.; Rivière, E.; Rogez, G.; Ghosh, S. K. *Inorg. Chem.* **2012**, *51*, 9159–9161.

(31) Mukherjee, S.; Joarder, B.; Manna, B.; Desai, A. V; Chaudhari, A. K.; Ghosh, S. K. *Sci. Rep.* **2014**, *4*, 5761.

(32) Zhu, K.; Chen, H.; Nishihara, S.; Liu, G.-X.; Ren, X.-M. *Inorg. Chim. Acta* **2009**, *362*, 4780–4784.

(33) Mukherjee, G.; Biradha, K. *Cryst. Growth Des.* **2011**, *11*, 5649–5658.

(34) Shen, Y.-C.; Li, Z.-J.; Cheng, J.-K.; Qin, Y.-Y.; Yao, Y.-G. *Inorg. Chem. Commun.* **2007**, *10*, 888–890.

(35) Wu, T.; Gong, Y. *Russ. J. Coord. Chem.* **2013**, *39*, 289–292.

(36) Hu, R.-F.; Zhang, J.; Kang, Y.; Yao, Y.-G. *Inorg. Chem. Commun.* **2005**, *8*, 828–830.

(37) Han, Z.-B.; Lu, R.-Y.; Liang, Y.-F.; Zhou, Y.-L.; Chen, Q.; Zeng, M.-H. *Inorg. Chem.* **2012**, *51*, 674–679.

(38) Papaefstathiou, G. S.; Vicente, R.; Raptopoulou, C. P.; Terzis, A.; Escuer, A.; Perlepes, S. P. *Eur. J. Inorg. Chem.* **2002**, *2002*, 2488–2493.

(39) Yang, E.-C.; Zhao, H.-K.; Ding, B.; Wang, X.-G.; Zhao, X.-J. *Cryst. Growth Des.* **2007**, *7*, 2009–2015.

(40) Zhang, X.-M.; Hao, Z.-M.; Zhang, W.-X.; Chen, X.-M. *Angew. Chem. Int. Ed.* **2007**, *46*, 3456–3459.

(41) Rybak, J.-C.; Schellenberg, I.; Pöttgen, R.; Müller-Buschbaum, K. *Zeit. Anorg. Allg. Chem.* **2010**, *636*, 1720–1725.

(42) Jiang, J.-Q.; Yang, C.-X.; Yan, X.-P. *Chem. Commun.* **2015**, *51*, 6540–6543.

(43) Hu, M.-C.; Wang, Y.; Zhai, Q.-G.; Li, S.-N.; Jiang, Y.-C.; Zhang, Y. *Inorg. Chem.* **2009**, *48*, 1449–1468.

(44) Schmieder, P.; Denysenko, D.; Grzywa, M.; Magdysyuk, O.; Volkmer, D. *Dalt. Trans.* **2016**, *45*, 13853–13862.

(45) Jones, L. F.; Rajaraman, G.; Brockman, J.; Murugesu, M.; Sanudo, E. C.; Raftery, J.; Teat, S. J.; Wernsdorfer, W.; Christou, G.; Brechin, E. K.; Collison, D. *Chem. Eur. J.* **2004**, *10*, 5180–5194.

(46) Biswas, S.; Tonigold, M.; Speldrich, M.; Kögerler, P.; Volkmer, D. *Eur. J. Inorg. Chem.* **2009**, 3094–3101.

(47) Wang, X.-L.; Qin, C.; Wu, S.-X.; Shao, K.-Z.; Lan, Y.-Q.; Wang, S.; Zhu, D.-X.; Su, Z.-M.; Wang, E.-B. *Angew. Chem. Int. Ed.* **2009**, *48*, 5291–5295.

(48) Collison, D.; McInnes, E. J. L.; Brechin, E. K. *Eur. J. Inorg. Chem.* **2006**, 2725–2733.

(49) Aromí, G.; Barrios, L. A.; Roubeau, O.; Gamez, P. *Coord. Chem. Rev.* **2011**, *255*, 485–546.

(50) Kostakis, G. E.; Xydias, P.; Nordlander, E.; Plakatouras, J. C. *Inorg. Chim. Acta* **2012**, *383*, 327–

331.

(51) Kallitsakis, M.; Loukopoulos, E.; Abdul-Sada, A.; Tizzard, G. J.; Coles, S. J.; Kostakis, G. E.; Lykakis, I. N. *Adv. Synth. Catal.* **2017**, *359*, 138–145.

(52) Loukopoulos, E.; Kallitsakis, M.; Tsoureas, N.; Abdul-Sada, A.; Chilton, N. F.; Lykakis, I. N.; Kostakis, G. E. *Inorg. Chem.* **2017**.

(53) Kurmoo, M. *Chem. Soc. Rev.* **2009**, *38*, 1353–1379.

(54) Murrie, M. *Chem. Soc. Rev.* **2010**, *39*, 1986–1995.

(55) Kostakis, G. E.; Perlepes, S. P.; Blatov, V. A.; Proserpio, D. M.; Powell, A. K. *Coord. Chem. Rev.* **2012**, *256*, 1246–1278.

(56) Idešicová, M.; Titiš, J.; Krzystek, J.; Boča, R. *Inorg. Chem.* **2013**, *52*, 9409–9417.

(57) Drulis, H.; Dyrek, K.; Hoffmann, K. P.; Hoffmann, S. K.; Weselucha-Birczynska, A. *Inorg. Chem.* **1985**, *24*, 4009–4012.

(58) Bencini, A.; Gatteschi, D. *Inorg. Chem.* **1977**, *16*, 2141–2142.

(59) Banci, L.; Benelli, C.; Gatteschi, D.; Mani, F. *Inorg.Chem.* **1982**, *21*, 1133–1136.

(60) Gatteschi, D.; Ghilardi, C. A.; Orlandini, A.; Sacconi, L. *Inorg. Chem.* **1978**, *17*, 3023–3026.

(61) Benelli, C.; Gateschi, D. *Inorg. Chem.* **1982**, *21*, 1788–1790.

(62) Benelli, C.; Gatteschi, D.; Speroni, G. *Inorganica Chim. Acta* **1984**, *90*, 179–183.

(63) Bencini, A.; Benelli, C.; Gatteschi, D.; Zanchini, C. *ESR spectra of low symmetry high spin cobalt(II) complexes. 8 [1]. Observation of ESR spectra of dichloro-tetrakispyrazole cobalt(II) doped into paramagnetic nickel(II) analogue*; Elsevier, 1980; Vol. 45.

(64) Bencini, A.; Benelli, C.; Gatteschi, D. *Inorg. Chem.* **1978**, *17*, 3313–3314.

(65) O'Keefe, B. J.; Steel, P. J. *Inorg. Chem. Commun.* **2000**, *3*, 473–475.

(66) Sun, M.; Zhou, W.-Z.; Wang, Y.-H.; Tan, H.-Q.; Qi, Y.-F.; Zang, H.-Y.; Li, Y.-G. *J. Coord. Chem.* **2016**, *69*, 1769–1779.

(67) Rajakumar, P.; Murali, V. *Tetrahedron* **2000**, *56*, 7995–7999.

(68) Macías, M. A.; Nuñez-Dallos, N.; Hurtado, J.; Suescun, L. *Acta Crystallogr. Sect. E Crystallogr. Commun.* **2016**, *72*, 815–818.

(69) Coles, S. J.; Gale, P. A. *Chem. Sci.* **2012**, *3*, 683–689.

(70) Dolomanov, O. V; Blake, A. J.; Champness, N. R.; Schröder, M. *J. Appl. Crystallogr.* **2003**, *36*, 1283–1284.

(71) Palatinus, L.; Chapuis, G. *J. Appl. Crystallogr.* **2007**, *40*, 786–790.

(72) Farrugia, L. J. *J. Appl. Crystallogr.* **1999**, *32*, 837–838.

(73) Sheldrick, G. M. *Acta Crystallogr. Sect. A Found. Adv.* **2015**, *71*, 3–8.

(74) Sheldrick, G. M. *Acta Crystallogr. Sect. A* **2008**, *64*, 112–122.

(75) Spek, A. L. *J. Appl. Crystallogr.* **2003**, *36*, 7–13.

(76) Macrae, C. F.; Edgington, P. R.; McCabe, P.; Pidcock, E.; Shields, G. P.; Taylor, R.; Towler, M.; Van De Streek, J. *J. Appl. Crystallogr.* **2006**, *39*, 453–457.

(77) Addison, A. W.; Rao, T. N.; Reedijk, J.; van Rijn, J.; Verschoor, G. C. *J. Chem. Soc. Dalt. Trans.* **1984**, 1349.

(78) Chilton, N. F.; Anderson, R. P.; Turner, L. D.; Soncini, A.; Murray, K. S. *J. Comput. Chem.* **2013**, *34*, 1164–1175.

For Table of Contents Use Only

Exploring the coordination capabilities of a family of flexible benzotriazole-based ligands using Cobalt (II) sources

Edward Loukopoulos,[a] Nicholas Chilton,[b] Alaa Abdul-Sada,[a] and George E. Kostakis*[a]

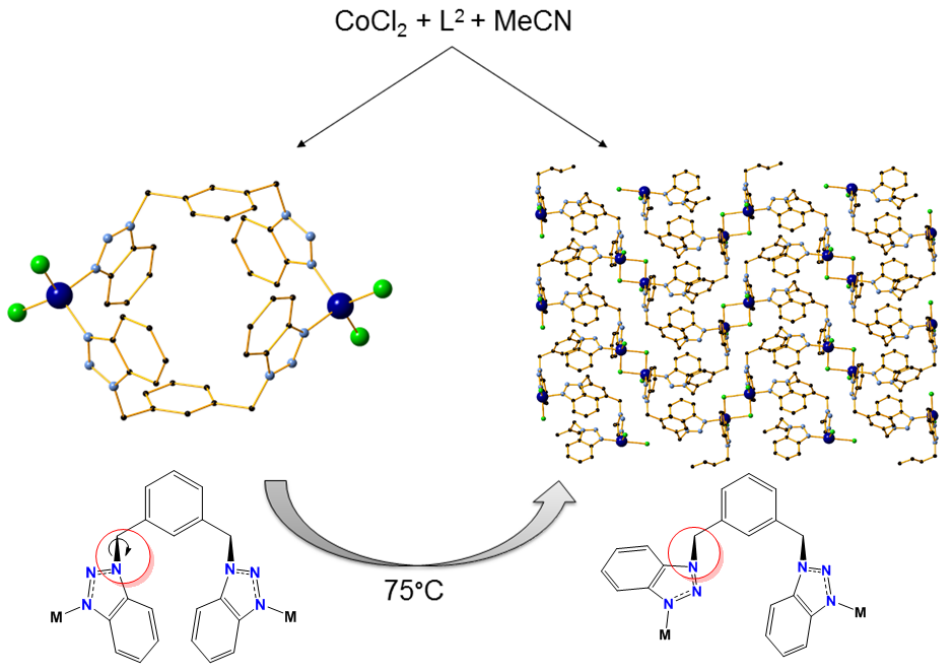

Employment of a family of semi-rigid benzotriazole-based ligands using Cobalt (II) salts reveal a large structural variety depending on synthetic parameters and ligand selection. Magnetic measurements, as well as a case of single-crystal to single-crystal transformation are also reported.